

# VIRTIS: The Visible and Infrared Thermal Imaging Spectrometer

G. Piccioni<sup>1</sup>, P. Drossart<sup>2</sup>, E. Suetta<sup>3</sup>, M. Cosi<sup>3</sup>, E. Ammannito<sup>4</sup>, A. Barbis<sup>3</sup>, R. Berlin<sup>6</sup>, A. Boccaccini<sup>1</sup>, G. Bonello<sup>1</sup>, M. Bouyé<sup>2</sup>, F. Capaccioni<sup>1</sup>, G. Cherubini<sup>3</sup>, M. Dami<sup>3</sup>, O. Dupuis<sup>2</sup>, A. Fave<sup>2</sup>, G. Filacchione<sup>1</sup>, Y. Hello<sup>2</sup>, F. Henry<sup>2</sup>, S. Hofer<sup>5</sup>, G. Huntzinger<sup>2</sup>, R. Melchiorri<sup>2</sup>, J. Parisot<sup>2</sup>, C. Pasqui<sup>3</sup>, G. Peter<sup>6</sup>, C. Pompei<sup>3</sup>, J.M. Ræss<sup>2</sup>, A. Semery<sup>2</sup>, A. Soufflot<sup>7</sup> and the VIRTIS Co-I team: A. Adriani<sup>4</sup>, F. Angrilli<sup>8</sup>, G. Arnold<sup>6</sup>, K. Baines<sup>9</sup>, G. Bellucci<sup>4</sup>, J. Benkhoff<sup>6</sup>, B. Bezard<sup>2</sup>, J.-P. Bibring<sup>7</sup>, A. Blanco<sup>10</sup>, M.I. Blecka<sup>11</sup>, R. Carlson<sup>9</sup>, A. Coradini<sup>4</sup>, A. Di Lellis<sup>1</sup>, T. Encrenaz<sup>2</sup>, S. Erard<sup>7</sup>, S. Fonti<sup>10</sup>, V. Formisano<sup>4</sup>, T. Fouchet<sup>2</sup>, R. Garcia<sup>12</sup>, R. Haus<sup>6</sup>, J. Helbert<sup>6</sup>, N.I. Ignatiev<sup>13</sup>, P. Irwin<sup>14</sup>, Y. Langevin<sup>7</sup>, S. Lebonnois<sup>15</sup>, M.A. Lopez Valverde<sup>16</sup>, D. Luz<sup>12</sup>, L. Marinangeli<sup>17</sup>, V. Orofino<sup>10</sup>, A.V. Rodin<sup>13</sup>, M.C. Roos-Serote<sup>18</sup>, B. Saggin<sup>19</sup>, A. Sanchez-Lavega<sup>20</sup>, D.M. Stam<sup>21</sup>, F. Taylor<sup>14</sup>, D. Titov<sup>22</sup>, G. Visconti<sup>23</sup> & M. Zambelli<sup>1</sup>

<sup>1</sup>*Istituto di Astrofisica Spaziale e Fisica Cosmica (INAF-IASF), via Del Fosso Del Cavaliere 100, I-00133 Rome, Italy*

*Email: giuseppe.piccioni@iasf.cnr.it*

<sup>2</sup>*Laboratoire d'Etudes Spatiales et d'Instrumentation en Astrophysique (LESIA), Observatoire de Paris/Meudon 5, Place Jules Janssen F-92195 Meudon cedex, France*

<sup>3</sup>*Galileo Avionica, via A. Einstein 35, I-50013 Campi Bisenzio (FI), Italy*

<sup>4</sup>*Istituto di Fisica dello Spazio Interplanetario (INAF-IFSI), via Del Fosso Del Cavaliere 100, I-00133 Rome, Italy*

<sup>5</sup>*Kayser-Threde GmbH, Wolfratshausener Strasse 48, D-81379 Munich, Germany*

<sup>6</sup>*German Aerospace Center (DLR) Institute of Planetary Exploration Planetary Physics, Berlin-Adlershof Rudower Chaussee 5, Geb. 16.16, D-12489 Berlin, Germany*

<sup>7</sup>*Institut d'Astrophysique Spatiale, Bâtiment 120 Université Paris-Sud, F-91405 Orsay cedex, France*

<sup>8</sup>*CISAS Università di Padova, via Venezia 1, I-35131 Padova, Italy*

<sup>9</sup>*Jet Propulsion Laboratory, MS 183-601 4800 Oak Grove Drive, Pasadena CA 91011, USA*

<sup>10</sup>*Università degli Studi di Lecce Dipartimento di Fisica, Via Arnesano, I-73100 Lecce, Italy*

<sup>11</sup>*Space Research Centre of Polish Academy of Science, Bartycka 18A, 00-716 Warszawa, Poland*

<sup>12</sup>*Département des Études Spatiales Institut de Physique du Globe de Paris 4, Avenue de Neptune F-94107 Saint Maur des Fossés cedex, France*

<sup>13</sup>*Space Research Institute (IKI), Profsojuznaja 84/32, 117997 Moscow, Russia*

<sup>14</sup>*University of Oxford, Dept. Physics Atmospheric, Oceanic and Planetary Physics, Clarendon Laboratory, Parks Road, Oxford OX1 3PU, UK*

<sup>15</sup>*Laboratoire de Meteorologie Dynamique, Jussieu, Box 99 F-75252 Paris cedex 05, France*

<sup>16</sup>*Instituto de Astrofísica de Andalucía (CSIC), Camino Bajo de Huétor, E-18080 Granada, Spain*

<sup>17</sup>*International Research School of Planetary Sciences, Dipartimento di Scienze Università d'Annunzio Viale Pindaro 42, 65127 Pescara, Italy*

<sup>18</sup>*Observatorio Astronómico de Lisboa Centro de Astronomia e Astrofísica da Universidade de Lisboa, Tapada da Ajuda P-1349-018, Lisboa, Portugal*

<sup>19</sup>*Politecnico di Milano, Polo di Lecco, via Marco D'Oggiono 18/A, I-23900 Lecco, Italy*

<sup>20</sup>*Dpto. Física Aplicada I Escuela Superior de Ingenieros Universidad del País Vasco, Alda. Urquijo s/n E-48013, Bilbao, Spain*

<sup>21</sup>*Astronomical Institute 'Anton Pannekoek' University of Amsterdam, Kruislaan 403 1098 SJ, Amsterdam, The Netherlands*

<sup>22</sup>*Max-Planck-Institute for Aeronomy, Max Planck Str. 2, D-37191 Katlenburg-Lindau, Germany*

<sup>23</sup>*Dept. of Physics, University of L'Aquila, via Vetoio Loc. Coppito, I-67010 Coppito, L'Aquila, Italy*

The VIRTIS imaging spectrometer built for ESA's Rosetta cometary mission is a versatile instrument that is also well-suited to Venus observations. The discovery of the near-IR windows in the atmosphere of Venus from ground-based observations in the 1980s showed that the surface of the planet can be studied via IR observations over the nightside. Imaging spectroscopy in the visible and near-IR can study the atmosphere from the uppermost layers down to the deepest levels. With its unique combination of mapping capabilities at low spectral resolution (VIRTIS-M) and high spectral resolution slit spectroscopy (VIRTIS-H), the instrument is ideal for making extensive IR and visible spectral images of the planet.

## 1. Scientific Objectives

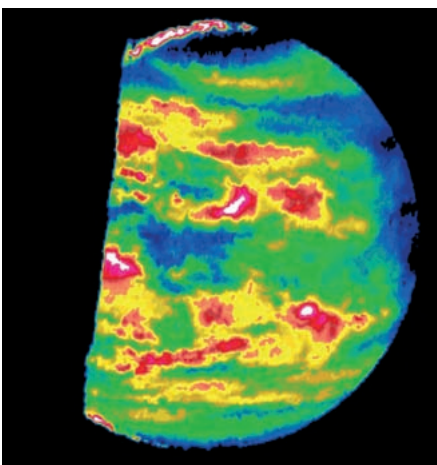
Observations of the nightside of Venus in the near-IR from Earth, first made by Allen & Crawford (1984), gave the first evidence of deep atmospheric sounding. These were followed by accurate spectroscopic measurements of the atmosphere with high spectral resolution spectroscopy (Bézard et al., 1990), including the water vapour and carbon monoxide that is important for thermochemical equilibrium studies (Kamp et al., 1988).

The first attempts at imaging spectrometry of the Venus nightside from space in the near-IR were made by Galileo's Near-IR Mapping Spectrometer (NIMS) in 1990 (Fig. 1; Carlson et al., 1991) and Cassini's Visual & IR Mapping Spectrometer (VIMS) in 1999 (Baines et al., 2000). These fast flybys indicated how powerful this method of investigation could be at Venus. Unfortunately, their brief durations strongly limited the investigations possible, particularly the meteorological evolution of the clouds. Observations of Venus with the VIRTIS new-generation imaging spectrometer is a unique opportunity to extend these investigations.

VIRTIS is able to produce day and nightside IR and visible spectra. The observation strategy for these scientific objectives is following the observing cases detailed in Section 5. The whole atmosphere is being observed from the mesospheric levels down to the surface (Taylor et al., 1997), and the surface itself is accessible to VIRTIS IR observations on the nightside. The main topics for VIRTIS science observations are:

- study of the lower atmosphere composition below the clouds and its variations (CO, OCS, SO<sub>2</sub>, H<sub>2</sub>O) from nightside observations (Collard et al., 1993). The 2.3 μm window (at high resolution with VIRTIS-H) gives access to accurate measurement of minor species. At shorter wavelengths, H<sub>2</sub>O is measurable with the lower spectral resolution of VIRTIS-M for mapping H<sub>2</sub>O variations, as done by NIMS/Galileo (Drossart et al., 1993). From these observations, correlation with volcanic or meteorological activity is being sought (some signatures of volcanic outgassing are related to minor-species variations, in particular for sulphur compounds).
- study of the cloud structure, composition and scattering properties (dayside and nightside). The different geometries of cloud reflections along with the spectral range of VIRTIS will constrain the cloud structure. The average structure is known from previous missions, but the temporal and spatial variabilities are less well documented. VIRTIS can sound the different layers and measure their optical thickness in the IR, and measure the upper layer on the dayside.
- cloud tracking in the UV (~70 km altitude, dayside) and IR (~50 km altitude, nightside). The correlation of UV and IR observations at different times, along with the 4-day cloud rotation period, gives access to the vertical variation of the wind field up to 70 km altitude.
- measurements of the temperature field with subsequent determination of the zonal wind in the altitude range 60–100 km (nightside). The 4–5 μm range is

Fig. 1. The Venus nightside at 2.3 μm, taken by Galileo (Carlson et al., 1991). The thermal emission from the deep atmosphere is modulated by the cloud structure of the deeper atmosphere. Cloudy regions appear in blue (lower emission), while bright regions (red) correspond to less cloud.



- sensitive to thermal structure, which can be retrieved (on the nightside) and compared with models (Roos et al., 1993). Such retrieval gives access to the vertical wind variations through cyclostrophic approximation.
- lightning search (nightside). Although tentative (there is no reliable information on the frequency of lightning on Venus), observations of transient lightning illumination are of high scientific interest, and is an ‘open search’ option for VIRTIS observations.
  - mesospheric sounding. Understanding the transition region between troposphere and thermosphere:
    - non-local thermodynamic equilibrium (non-LTE) O<sub>2</sub> emission (night/dayside) at 1.27 μm (95–110 km; Drossart et al., 1993). As observed from the ground and NIMS/Galileo, these emissions have spatial and temporal variabilities, which make them of high interest for accurate spatial mapping by VIRTIS.
    - CO<sub>2</sub> fluorescence (dayside). Non-LTE emissions at 4.3 μm (>80 km; Roldan et al., 2000) on limb scans by Galileo provide important information on the physics of the upper atmosphere through the collisional/radiative equilibrium sounded through the CO<sub>2</sub> band.
    - limb observations (CO, CO<sub>2</sub>): atmospheric vertical structure (>60 km) (day/nightside).
  - search for variations related to surface/atmosphere interaction, dynamics, meteorology and volcanism. Global observation or partial observations at a regional scale on a temporal scale of one Venusian day is allowing the search for correlations between different physical processes.
  - temperature mapping of the surface and searching for hot spots related to volcanic activity. NIMS/Galileo observations of Io showed that lava lakes are easily detected on a planet by imaging spectroscopy. Even if the atmosphere of Venus precludes the clear detection of free lava, a temperature anomaly could be a signature of some volcanic activity. This has never been attempted with the spatial/temporal performance of an instrument like VIRTIS.
  - search for seismic waves from the propagation of acoustic waves amplified in the mesosphere by looking for high-altitude variations of pressure/temperature in the CO<sub>2</sub> 4.3 μm band (Artru et al., 2001). Although clearly a challenge, it is one of the tentative science objectives that would be of primary scientific importance if detected. Gravity waves also have signatures in the IR mesospheric emissions accessible to VIRTIS. Very little is known about wave activity in the upper atmosphere of Venus.

These objectives during the nominal Venus Express mission mean that VIRTIS is providing a very broad scientific return.

## 2.1 Overview

Although with some modifications, VIRTIS for Venus Express is essentially identical to the instrument carried by Rosetta (Coradini et al., 1998). It is an imaging spectrometer with three focal planes and two channels. The mapping channel has two 2-D focal planes: visible (0.25–1 μm) and IR (1–5 μm). The spectroscopic channel has a single aperture but provides high-resolution spectra at 2–5 μm. The IR focal plane array (FPA) uses HgCdTe arrays of 270 x 438-pixel detectors designed to provide high sensitivity and low dark current (about 1 fA at 80K), with a read noise lower than 300 e<sup>-</sup>.

As on Rosetta, the electronic module and data handling support unit were built in Germany (Kayser-Threde for hardware, DLR for software and management), VIRTIS-M by Galileo Avionica Florence-Italy and VIRTIS-H by Paris Observatory, France. Integration and programme management were in

## 2. Instrument Description

Table 1. VIRTIS principal characteristics.

	<i>VIRTIS-M Visible</i>	<i>VIRTIS-M Infrared</i>	<i>VIRTIS-H</i>
Spectral range (nm)	280 – 1100	1050 – 5130	1840 – 4990
Spectral resolution $\lambda/\Delta\lambda$	150 – 500	100 – 500	1300 – 3000
Spectral sampling (nm) [note 1]	1.89	9.47	0.6
Field of view (mrad x mrad)	64 (slit) x 64 (scan)		0.44 x 1.34
Max spatial resolution ( $\mu\text{rad}$ )	250 (slit) x 250 (scan)		–
Image size, full FOV high resolution (pixels)	256 x 256		–
noise equivalent spectral radiance (central band, $\text{Wm}^{-2}\text{sr}^{-1}\mu\text{m}^{-1}$ )	$1.4 \times 10^{-2}$	$1.2 \times 10^{-4}$	$1.2 \times 10^{-4}$
Telescope	Shafer Telescope	Shafer Telescope	off-axis parabolic mirror
Pupil diameter (mm)	47.5		32
Imaging F#	5.6	3.2	2.04
Etendue ( $\text{m}^2 \text{sr}$ )	$4.6 \times 10^{-11}$	$7.5 \times 10^{-11}$	$0.8 \times 10^{-9}$
Slit dimension (mm)	0.038 x 9.53		0.029 x 0.089
Spectrometer	Offner Relay	Offner Relay	Echelle spectrometer
Detectors	Thomson TH7896 CCD	HgCdTe [note 2]	HgCdTe [note 2]
Sensitivity area format	508 x 1024	270 x 436	270 x 436
Pixel pitch (mm)	19	38	38
Operating temperature (K)	150 – 190	65 – 90	65 – 90
Spectral range ( $\mu\text{m}$ )	0.25 – 1.05	0.95 – 5.0	0.95 – 5.0
Mean dark current	< 1 e/s	< 2 fA @ 90K	< 2 fA @ 90K

Notes. 1: depends on selected mode of operation; the maximum value is shown. 2: VIRTIS-M and VIRTIS-H use identical IR detectors.

Florence. There are differences between the Rosetta and Venus Express instruments owing to the very different targets: the cold nucleus of a comet and the hot planetary atmosphere of Venus. The Venus Express design improves thermal dissipation, adapts the integration timescale and reduces the repetition time between successive observations. Table 1 provides the instrument's main characteristics.

The output from VIRTIS-M (Fig. 2) can be considered to be a large set of stacked monochromatic 2-D images (spatial direction in the x-y plane) in the range 0.25–5  $\mu\text{m}$  (l axis), at moderate spectral resolution. The VIRTIS-H field-of-view is centred in the middle of the -M image and provides spectra at high spectral resolution in this small portion of the image.

As shown in Fig. 3, VIRTIS consists of four Modules: the Optics Module (OM) containing the -M and -H Optical Heads; the two Proximity Electronics Modules (PEM-M and PEM-H) and the Main Electronics Module (ME).

The Optics Module is externally mounted on the -X panel of the spacecraft with the Optical Heads co-aligned and boresighted in the +Z direction. Both optical systems have their slits parallel to the Y axis; VIRTIS-M can point and scan by rotating the primary mirror around the Y-axis. Two views of the Optics Module are shown in Figs. 4 and 5.

VIRTIS-M uses a Si CCD (Thomson TH7896) to image from 0.25  $\mu\text{m}$  to 1  $\mu\text{m}$  and an HgCdTe IR focal plane array (IRFPA, Raytheon) to image from 1  $\mu\text{m}$  to 5  $\mu\text{m}$ . VIRTIS-H uses the same HgCdTe IRFPA to perform spectroscopy in selected bands from 2  $\mu\text{m}$  to 5  $\mu\text{m}$  (see Table 1).

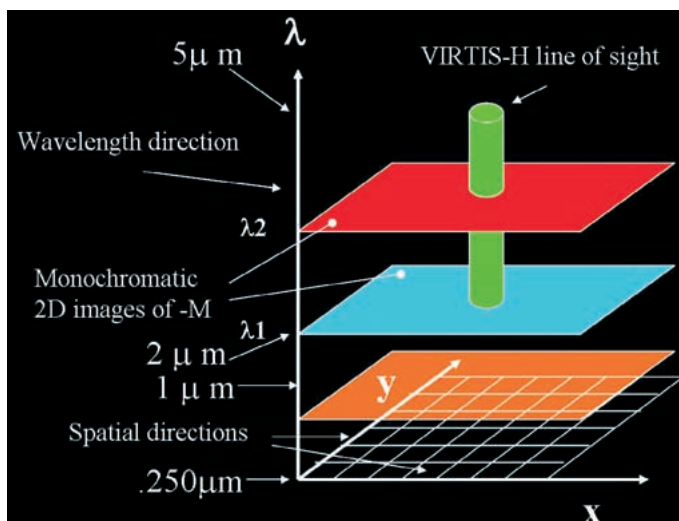


Fig. 2. The output from VIRTIS-M can be considered to be a large set of stacked monochromatic 2-D images (spatial direction is in the x-y plane) in the range 0.25–5  $\mu\text{m}$  ( $\lambda$  axis), at moderate spectral resolution. The VIRTIS-H field-of-view centred in the -M image provides spectra at high spectral resolution in this small portion of the frame.

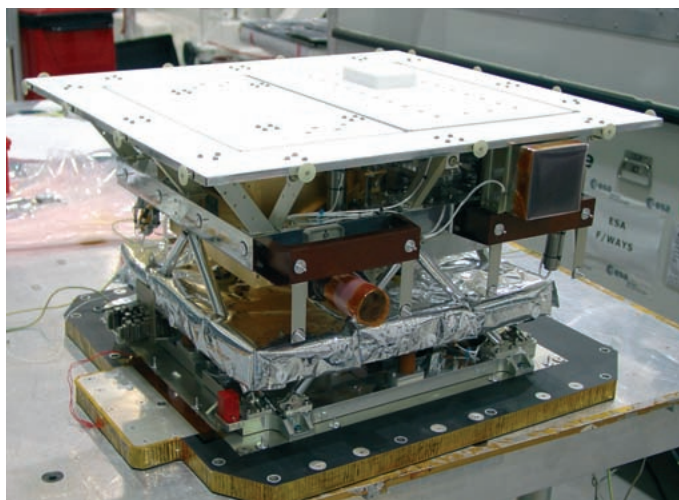


Fig. 4. The Optics Module mounted on its support structure shortly before installation of the multi-layer insulation and final integration on the spacecraft at Alenia Spazio in Turin. The -M channel is at right top; the -H channel is at left top.

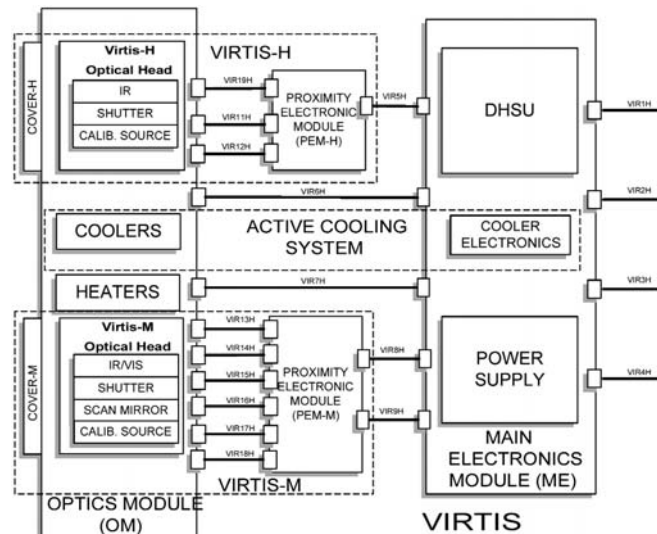


Fig. 3. The VIRTIS functional block diagram. DHSU: Data Handling and Support Unit.

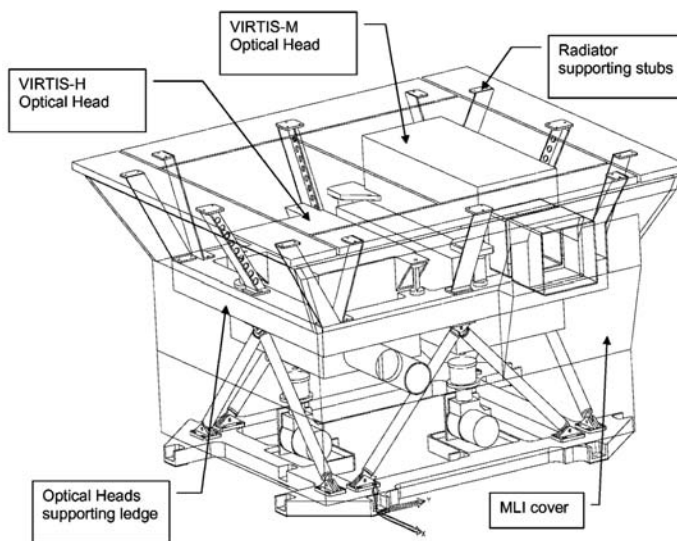


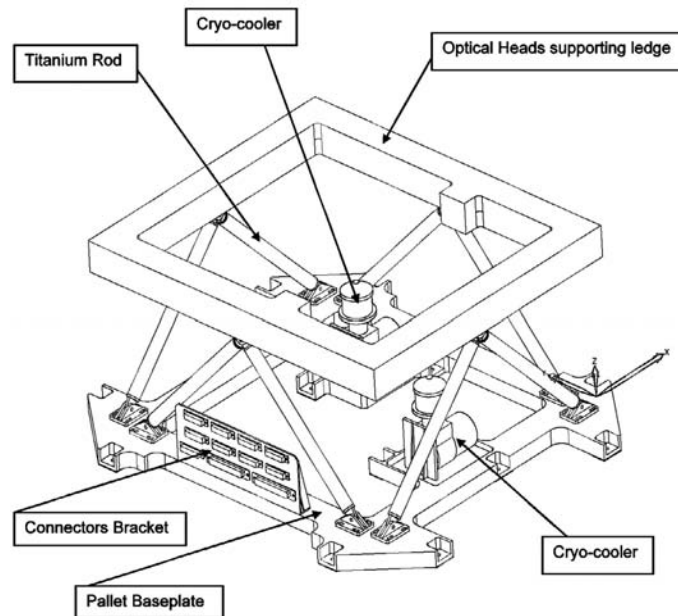
Fig. 5. The Optics Module structure. From a thermal-mechanical point of view, the structure is divided into two (top and bottom), at very different temperatures. The cold side (top) is directly coupled to the radiator (and cold space) and the warm side (bottom) is the baseplate in contact with the spacecraft.

The electronics boards required to drive the CCD and the two IRFPAs and to acquire housekeeping information from the optical heads are housed in the PEMs. VIRTIS-ME controls the interface with the PEMs and the spacecraft, controls the cryocoolers and the power conditioning and distribution, and performs all the digital data-handling.

The IR detectors require active cooling to minimise the detector dark current owing to the thermally generated Johnson noise. Their operating temperature is typically 80K.

In order to minimise the thermal background radiation seen by these two IRFPAs, the Optics Module is divided into two parts:

Fig. 6. The baseplate Pallet with the two cryocoolers and the connector bracket, the eight titanium rods fixing the Cold Box mounting ledge on the baseplate, and the empty ledge to which the two Optical Heads are rigidly connected.



- the Pallet directly interfaces with the warm spacecraft (i.e. it is thermally controlled by the spacecraft) and houses the two cryocoolers.
- the Cold Box structure is rigidly mounted to the much warmer Pallet but thermally insulated from it. It contains the cold detectors and the two Optical Heads and is thermally disconnected from the spacecraft and passively cooled below 150K by radiating one of its surfaces towards cold space. The optical heads are mounted on the Cold Box Ledge.

Two cold fingers connect the two active coolers inside the Pallet to their corresponding IRFPAs inside the Cold Box; they must maximise the thermal pathway from the coolers to the IRFPAs while remaining mechanically pliant. In contrast, the stand-off insulators (eight titanium rods) connecting the Cold Box to the baseplate of the Pallet minimise the thermal pathway between the warm spacecraft and the cold optical subsystems while remaining mechanically rigid. In this way, the structure and the delicate subsystems that it supports were not only guaranteed to survive launch vibrations, but the structure also helps in minimising the usual thermal gradients that adversely affect the alignment of low-temperature optical systems.

Since the CCD is a frame-transfer device and the IRFPAs are direct injection devices, exposure times can be controlled electronically. However, measurement of the detector dark current plus background radiation requires calibration shutters to be placed at the entrance light-limiting slit of each spectrometer (telescope background contribution is negligible because of its low temperature and the narrow width of the slit).

Each VIRTIS-M and -H channel has a cover to protect the instrument from direct Sun illumination and to preserve the cold environment inside the Cold Boxes when the Sun is within the field of view when VIRTIS is not operational. Each cover has an emergency actuator to force it open in case of malfunction.

The covers are machined as retro-reflectors for in-flight calibration. This feature also came in useful during ground-testing of the instrument, especially when it was not on an optical test bench.

## 2.2 The team

VIRTIS is the result of the joint efforts of several scientific institutes and companies in different European countries. The institutes involved in the hardware development, calibration and testing were:

- Istituto di Astrofisica Spaziale e Fisica Cosmica (IASF), Rome, Italy;
- Laboratoire d'Etudes Spatiales et d'Instrumentation en Astrophysique (LESIA), Observatoire de Paris, Meudon, France;
- Galileo Avionica (GA), Florence, Italy (VIRTIS prime contractor);
- Institut für Planeteterkundung DLR, Berlin, Germany;
- Kayser-Threde GmbH, Munich, Germany;
- Istituto di Fisica dello Spazio Interplanetario (IFSI), Rome, Italy;
- Institut d'astrophysique Spatial (IAS), Orsay, France;
- Università di Lecce, Italy;
- CISAS-DIM, Università di Padova, Italy.

The tasks were defined on the basis of the VIRTIS-Rosetta structure. The general sharing of responsibility among countries was:

VIRTIS-M	Italy
VIRTIS-H	France
Optics Module structure	Italy
Active cooling subsystem	Italy
Main Electronics Module	Germany
Cover subsystem	Italy
Ground Support Equipment	Italy
Shutter Unit	France
Sunshields	Italy

The VIRTIS prime contractor is Galileo Avionica, responsible, apart from the overall integration, for the production and testing of VIRTIS-M, the Optical Module Structure and the Sunshields for both -M and -H.

The two Co-Principal Investigators are G. Piccioni (INAF-IASF Rome) and P. Drossart (LESIA Paris). Forty Co-Investigators from ten countries are participating in the data analysis.

## 2.3 The Optical Module structure

The OM's main function is to provide mechanical support for the VIRTIS optical subsystems while maintaining them at an operating temperature below 150K and the two IR focal planes at 80K. To achieve this, the OM is divided into two principal functional parts (Fig. 6): a warm enclosure and a cold enclosure (the 'Cold Box').

The warm enclosure includes the OM baseplate, the Inter-Unit Harness brackets, the Active Cooling Subsystem (a pair of cryocoolers, one each for -M and -H) and the structural truss that thermally insulates the upper Cold Box from the baseplate. The Cold Box includes the two optical subsystems, mounted on a cold ledge that also supports the cover mechanisms, the two baffles and the passive cooling hardware.

The mechanical interface with the spacecraft is the OM baseplate connected to a special supporting structure provided by the Venus Express spacecraft (not present on Rosetta). A set of four thermal pipes in the structure is dedicated to the thermal power dissipation of the VIRTIS cryocoolers. In this way, the power generated on the baseplate, mostly from the cryocoolers, is conductively dissipated to deep space through a dedicated radiator.

The cryocoolers' cold-tips are conductively connected to the VIRTIS IR detectors via flexible thermal straps.

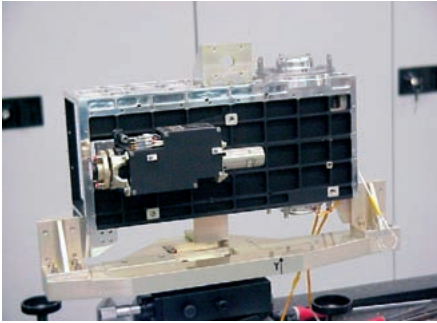


Fig. 7. VIRTIS-M during assembly. The grating is in the centre, the FPAs are on the right-hand side and the slit is on the left.

The passive cooling to keep the -H and -M temperatures below 150K consists of a primary radiator, conductively connected to the ledge, and two secondary radiators, one each for -M and -H. The three radiators are placed on the spacecraft's -X-axis, looking at cold space; their overall envelope is about 590 x 650 mm.

The primary radiator refrigerates the ledge to slightly higher than the instrument's temperature, by dissipating the heat from the truss and from part of the internal cabling. The secondary radiators are each mounted directly on top of the instruments.

The Cold Box and the warm enclosure are externally covered with multi-layer insulation (MLI). An MLI blanket separates, from a radiative point of view, the Cold Box from the warm enclosure.

The low-conducting heat load between the cold and warm enclosures is achieved by mounting the Cold Box on eight titanium hollow struts. The number and attachment positions were selected to avoid distortion upon cooling from room temperature. All of the struts are blanketed with MLI to reduce the thermal load and avoid differential heating of the cold ledge.

The heat flow through the Cold Box is small enough that the VIRTIS optical subsystems are mounted inside an essentially isothermal cavity. To help maintain this isothermal cavity, the covers and actuators for the -M and -H entrance ports are inside the Cold Box, between the optical subsystems and the external MLI blanket.

## 2.4 VIRTIS-M

VIRTIS-M is the mapping spectrometer of VIRTIS. It consists of the -M optical head inside the OM and the PEM-M proximity electronics close to it but residing in the spacecraft in a warm thermally controlled environment. The optical head consists of the telescope and spectrometer that are shared by the visible and IR channels and then naturally co-aligned into one unique optical axis (Fig. 7).

### 2.4.1 Telescope

The Shafer-type telescope is the combination of an inverted Burch telescope and an Offner relay. The Offner relay takes the curved, anastigmatic virtual image of the inverted telescope and makes it flat and real without losing the anastigmatic quality. Coma optical aberration is eliminated by putting the aperture stop near the centre of curvature of the primary mirror, thus making the telescope monocentric. The result is a telescope system that relies only on spherical mirrors yet remains diffraction-limited over an appreciable spectrum and all the vertical field (slit direction).

The horizontal field is realised by rotating the mirror of the Shafer telescope around an axis parallel to the Y-axis of the spacecraft. The optical system is not diffraction-limited over the overall field but the optical quality is still sufficient.

### 2.4.2 Spectrometer

The imaging spectrometers of the Cassini (VIMS) and Mars Express (OMEGA) Bibring et al., 2004) missions required separately housed co-aligned instruments to cover the visible and IR spectra. The VIRTIS-M Offner spectrometer not only does away with redundant optical systems, but also eliminates the need for collimators, camera objectives and beam splitters, thereby simplifying fabrication and minimising volume and mass. However, a grating spectrometer that does not rely on a collimator and camera objective requires perfect matching with its collecting telescope. Not only must they have matching F-numbers, but the telescope must be telecentric or have its exit pupil positioned on the grating. The Shafer telescope is matched to the Offner spectrometer because both are telecentric. This means that the entrance pupil is positioned in the front focal length of the optical system 750 mm in front of the primary mirror.

The VIRTIS-M spectrometer grating does away with the beam splitter by realising two different groove densities (Piccioni et al., 2000) on a single substrate (Fig. 8). Since the pupil optics conjugate is on the grating, the same spectral beam splitting is performed for each FOV angle. The grating profiles are holographically recorded into a photoresist coating and then etched with an ion beam. Using various masks, the grating surface can be separated into different zones with different groove densities and different groove depths. The ‘V’ regions (inner parts), which make up the central 30% of the conjugate pupil area, correspond to the higher groove density needed to generate the higher spectral resolution required in the ‘visible’ channel extending from the UV to the near-IR. The smaller pupil area allows the visible channel to operate partially coherently and achieve a smaller point spread function.

The IR channel (outer part) has a pupil area equal to 70% of the total. Since the IR channel does not require such high resolution as the visible channel, it was decided to accept for this channel a lower Modulation Transfer Function (MTF), caused by the visible zone’s obscuration of the IR pupil. In the visible channel, the diffraction spot diameter is smaller than the pixel size, so the main factor for the optical quality is the optical system aberrations. Conversely, in the IR channel, the optical quality is affected mainly by the diffraction. Furthermore, the central obscuration in the IR reduces the diffraction MTF by a further 10%.

A laminar grating with a rectangular groove profile is used for the visible channel pupil zone to enable two different groove depths to alter the grating efficiency spectrum and compensate for low solar energy and low CCD quantum efficiency in the UV and near-IR regions. The resulting efficiency, improves the instrument’s dynamic range by increasing the signal-to-noise ratio (SNR) at the extreme wavelengths and preventing saturation in the central wavelengths.

To minimise the effects of background radiation emitted in the form of photons with wavelengths longer than  $4.2\ \mu\text{m}$ , both IRFPAs have to be protected by spectral blocking filters with cut-off wavelengths at  $5.1\ \mu\text{m}$ . In addition, VIRTIS-M also requires prevention of the superimposition of higher diffraction orders coming from the grating (VIS and IR channels), by inserting a dedicated long-pass filter in the optical path.

Since the  $4.2\text{--}5.1\ \mu\text{m}$  background radiation cannot be filtered within the same spectral band in which the data are collected, the spectrometer must be cooled to below 150K.

#### 2.4.3 PEM-M

The PEM-M, housed in the spacecraft, contains all the electronics needed to interface the Main Electronics, to drive the FPAs, the scan mirror and the cover mechanism and to perform the acquisition and conversion of the science and housekeeping data.

The electronics package consists of a mother board and four daughter boards, of which two are committed to the visible channel, one to the IR channel and one to the scan and cover control units. Fig. 9 shows the PEM-M block diagram together with the Optical Head devices.

The interface circuits with the Main Electronics are located on the mother board and are implemented with monodirectional balanced interfaces.

The visible channel comprises four main blocks: data acquisition; analogue-to-digital converter (ADC); the CCD bias and drivers; the FPGA.

The data-acquisition block is based on a low-noise amplifier chain containing a correlated double-sampling circuit to eliminate every uncertainty caused by the reset noise. The ADC (7805ALPRP) ensures a 16-bit resolution with a  $10\ \mu\text{s}$  conversion time.

The CCD phase drivers translate the patterns generated by a dedicated ASIC to MOS levels in order to drive correctly the large capacitive loads of the CCD rows and columns with low power consumption.

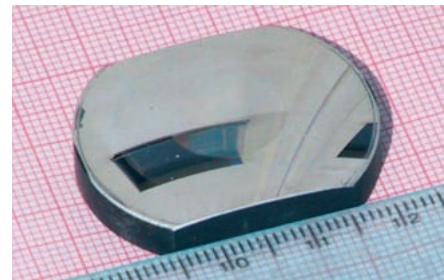
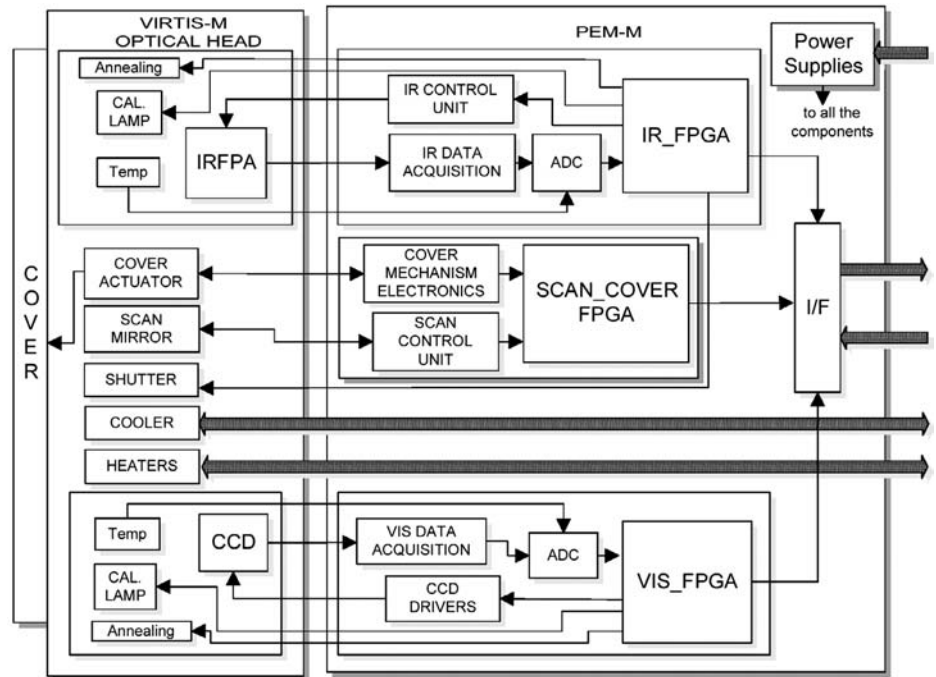


**Fig. 8.** The VIRTIS-M grating used for the development model. The two inner regions are for the visible range, the external one is for IR. The dispersion axis is roughly along the ruler. The surface geometry is convex.

Fig. 9. VIRTIS-M block diagram. The Optical Head mechanisms and devices are on the left side, while the electronics (PEM-M) are represented on the right with their block structure.



The main function of the FPGA (ACTEL RT14100) is to initialise the ASIC timing generator, and to control the ME command interpreter, the data transmission, the calibration source and annealing heaters.

From a functional point of view, the IR channel is very similar to the visible channel. The IRFPA control unit and acquisition chain are simpler, with all the electronics on one board. The IR FPGA (ACTEL RT14100) is dedicated to controlling the shutter mechanism.

The acquisition, conversion and transmission of the VIRTIS-M housekeeping data (temperature, voltage and current measurements) are divided between the visible and IR channel.

The scan unit board performs accurate positioning of the primary mirror to the commanded angle. The scanning movement is done step by step. Each step moves a new portion of the field of view of the interferometer slit. The control is accomplished using a two-phase DC brushless motor to provide the torque; the current flowing in the stator windings produces a torque at the permanent magnet rotor. The Inductosyn position transducer provides 10 arcsec accuracy. It is essentially a variable coupling transformer, the magnitude of which varies according to the position of the rotating element.

The control logic interface is based on an ACTEL FPGA (RT14100) receiving scan unit commands via a synchronous serial link and calculating the position error. This FPGA also contains the cover mechanism control logic, which actuates the cover by a stepper motor. The end positions (open and closed) are computed step-by-step starting from a mechanical reference (end-stop). In addition, two Hall-effect sensors (HESs) monitor the position reached by the cover after the opening or closing command. The Cover Mechanism Electronics include two drivers for the windings of the stepper motor and the front end for the two HESs. Two different supply lines close or open the cover, then power-off the motor and continue to monitor the cover position by the HES outputs.

#### 2.4.4 Focal Plane Array: visible detector

The visible FPA is based on the Thomson-CSF TH7896 CCD detector. It uses a

buried channel design and two poly-silicon N-MOS technology to achieve good electro-optical performance. It includes a multi-pinned phase boron implant to operate fully inverted and to reduce substantially the surface dark current, residual images after strong exposure and other effects due to ionising radiation. The TH7896M is a full-frame image sensor with 1024 x 1024 sensitive elements, two registers and four outputs, but it is used as a frame-transfer device, shielding half the sensitive area that works as a memory section. Only one horizontal register and one output are actually used.

To obtain sensitivity to 250 nm, there is a UV-coating on columns 1–112. This coating emits light at approximately 540–580 nm when excited with wavelengths shorter than 450 nm. It is transparent in the visible and near-IR, and does not significantly influence quantum efficiency in this portion of the spectrum.

In order to generate the required information (to meet the instantaneous FOV of 250  $\mu$ rad and to have the same pixel size in the IR and visible detectors), 2 x 2 binning is implemented at the detector level. This approach achieves the required pixel size with a less expensive solution; a 38  $\mu$ m pixel size is feasible but would require a custom design.

Effects on charge transfer efficiency owing to radiation-induced dark current spikes and residual bulk image are minimised when operating at very low temperatures. Proton interactions with the silicon lattice produce deep-level traps that begin to freeze out at 200K and become inactive at 160K. In fact, once filled with electrons, these traps remain filled owing to the long emission time constant. The challenge is then to keep the CCD temperature as close as possible to that of the Cold Box while preventing degradation of the charge transfer efficiency owing to buried channel freeze-out and bulk trap characteristics. The thermal-mechanical design of the FPAs fulfils this goal.

The detector is also equipped with two ordering filters with a boundary at band 215 (680 nm) in order to attenuate the higher orders of the visible grating region.

#### 2.4.5 Focal Plane Arrays: IR detectors

The IR detectors used in VIRTIS-H and VIRTIS-M are based on a 2-D array of IR-sensitive photovoltaic mercury-cadmium-tellurium (HgCdTe). The growth technique for the crystal is critical for high-performance FPAs because structural defects in the material result in defective photodiodes. The preferred growth technique for producing the best material, in terms of crystalline quality, electrical uniformity and reproducibility, is the liquid or molecular epitaxy process. These devices have the potential to operate at a higher temperature than the more established indium antimonide (InSb) detectors owing to dark current reduction by a factor of 10 or more.

The detector is manufactured by Raytheon Infrared Operations (Santa Barbara, USA). The charge trans-impedance amplifier technology used on this detector is the best solution when external low background flux ( $6 \times 10^7$  to  $2 \times 10^{11}$  photon  $\text{cm}^{-2} \text{s}^{-1}$ ) has to be detected, as is the case for Rosetta's comet and the Venus nightside.

The array is formed through hybridisation of mercury-cadmium-telluride (MCT) material with dedicated Si CMOS. The device is a MCT-Si hybrid array of 270(w) x 436(h) 38 $\mu$ m MCT photodiodes with line and column spacing of 38  $\mu$ m between diode centres, a spectral wavelength range from 0.95  $\mu$ m up to 5  $\mu$ m and an operating temperature of 80K. The device has a flatpack encapsulation, adapted to take a pressure-bonded window and with an internal filter to separate the grating's higher orders and to suppress background radiation.

The detector is packaged into a housing which includes an optical window and provides mechanical, thermal and electrical interfaces for its integration on the VIRTIS-H and -M FPAs.

The VIRTIS-M filter window is used to stop the superimposition of higher diffraction orders from the grating and also to eliminate/reduce the background thermal radiation due to the temperature of the instrument housing. The window is covered with anti-reflection coating optimised in the 1–5.1  $\mu\text{m}$  region. Five segment filters are coated on to the window with the following bandpasses:

- 1st region: 0.9–1.6  $\mu\text{m}$ ;
- 2nd region: 1.2–2.5  $\mu\text{m}$ ;
- 3rd region: 2.4–3.75  $\mu\text{m}$ ;
- 4th region: 3.6–4.4  $\mu\text{m}$ ;
- 5th region: 4.3–5.0  $\mu\text{m}$ .

#### 2.4.6 VIRTIS-M modes

The possible modes for VIRTIS-M are summarised in Table 2. The overall data rate and volume depend essentially on the selected modes for -M because -H does not much affect the rate (unless special testing modes are used, involving the transfer of the full frame).

## 2.5 VIRTIS-H

The VIRTIS-H optical design is based on a cross-dispersion concept (Fig. 10). Its beam etendue is  $0.8 \times 10^9 \text{ m}^2 \text{ sr}$  for an instantaneous FOV of  $0.58 \times 1.74 \text{ mrad}$ . A mean resolution of  $\lambda/\Delta\lambda = 2000$  in the spectral region 2–5  $\mu\text{m}$  gives about 3500 spectral elements. The 32 mm entrance pupil is placed near the F/1.6 off-axis parabolic telescope. The magnification of the spectrometer (between the slit and the detector) is 1.3, so the slit image covers 3 pixels, although 5 pixels are summed per spectral element to avoid any signal loss.

To reach the SNR specifications, the spectrometer is cooled below 150K and the detector is cooled to 80K.

VIRTIS-H consists of four main parts: an afocal module, the dispersion module, an objective and a focal plane assembly. The afocal module is composed of two aluminium off-axis parabolas (telescope and collimator) with the same focal plane in which the entrance slit is placed. A shutter near the entrance slit allows background measurements. This assembly is mounted on a bench made with the same material as the mirrors; this makes a compact low-straylight achromatic system that can be adjusted in the visible at room temperature.

The dispersion module consists of a prism and a reflection grating. Eight orders of the grating (6–13), perpendicularly separated by a magnesium oxide prism, are used (Table 3). The grating is split into two differently blazed parts to allow a smoother efficiency profile along each order.

Table 2. VIRTIS-M modes.

	Number of pixels		Binning		Detectors
	spectral	spatial	spectral	spatial	
NOMINAL_3X4_FULL_WIN	144	64	3	4	VIS + IR
VIS_ONLY_1X4	288	64	1	4	VIS
IR_ONLY1X4	288	64	1	4	IR
HIGH_SPECTRAL1X4_FULL_WIN	432	64	1	4	VIS+IR
HIGH_SPATIAL_3X1_FULL_WIN	144	256	3	1	VIS+IR
ALL_PIX_FULL_WIN	432	256	1	1	VIS+IR
REDUCED_SLIT_3X1	144	64	3	1	VIS+IR
ALTER_IR_ONLY_1X4	288	64	1	4	IR

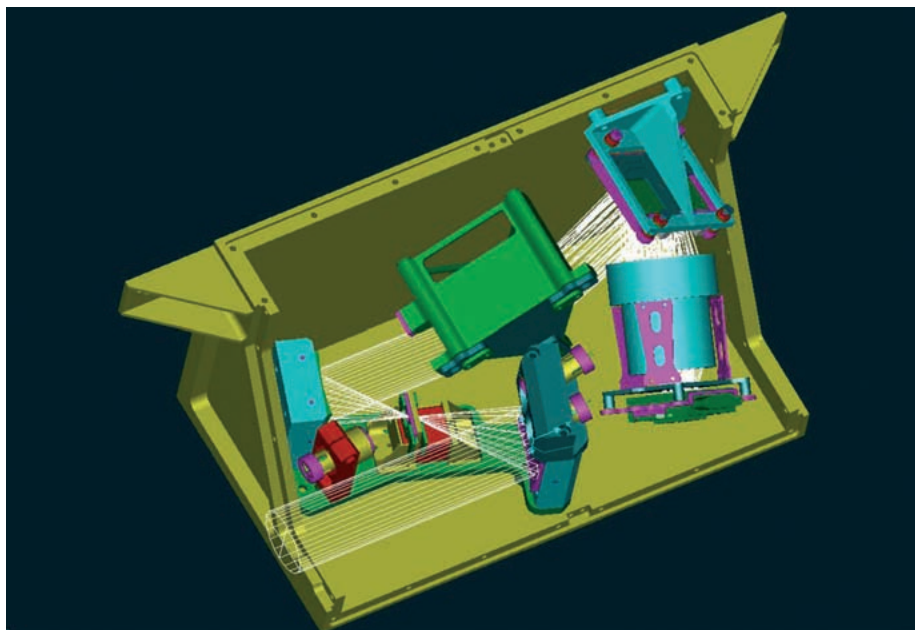


Fig. 10. A simplified view of the VIRTIS-H optical scheme.

The F/2 objective is composed of two silicon and one germanium lenses. The entrance face of the first Si lens is elliptical ( $e = -0.1171$ ). As it is close to the grating (the instrument white pupil), the objective spherical aberration is drastically reduced. The position of the white pupil makes the objective and the system strongly telecentric.

The FPA includes a two-zone filter that isolates the lower order (4.0–5.0  $\mu\text{m}$ ) from the others. The main goal of this filter is to remove the thermal background in the shorter wavelengths, thereby increasing the SNR in this spectral region.

The overall FPA can be adjusted in tilt and focus with respect to the objective.

Since the 4.0–5.0  $\mu\text{m}$  background radiation cannot be filtered within the same spectral band in which the data are collected, the spectrometer must be cooled to below 150K to cope with the low signal levels.

The straylight is reduced via several baffles and black-anodised mechanical mounts in the spectrometer. A baffle is placed between the spectrometer entrance and the telescope, and another one near the entrance slit. The objective and the FPA are linked using baffles.

The instrument is optically adjusted using hard wedges, which makes it very stable. First, the afocal whole (telescope-slit-collimator) was adjusted at room temperature using wedges on the telescope and the collimator; the material uniformity means there is no misalignment at the working temperature of this system. The IR adjustment at the working temperature of the overall instrument was made using wedges on the FPA and the grating.

The optical quality of the instrument is very good because it is strongly diffraction-limited in the overall spectral band. Owing to the presence of a grating, the spectral resolution ( $\lambda/\Delta\lambda$ ) varies in each order between 1500 and 2900.

VIRTIS-H uses the same IR detector as VIRTIS-M but, owing to the different designs of the two channels, the detector is used rather differently. VIRTIS-H is a high-resolution spectrometer and does not perform imaging. Its IR detector acquires spectra spread over its surface, so only a portion of the pixels contains useful scientific data. The eight spectral orders are spread over the entire surface matrix. In each spectral order the spectrum covers  $432 \times 5$  pixels (where 5 pixels represent the image of the slit size when imaged on the detector).

Table 3. VIRTIS-H grating orders.

Order ( $\mu\text{m}$ )	$\lambda_{min}$	$\lambda_{max}$
Order 0	4.00342	4.98660
Order 1	3.43527	4.28712
Order 2	3.00538	3.75714
Order 3	2.67117	3.34079
Order 4	2.40335	3.00673
Order 5	2.18426	2.73313
Order 6	2.00126	2.50554
Order 7	1.84486	2.31273

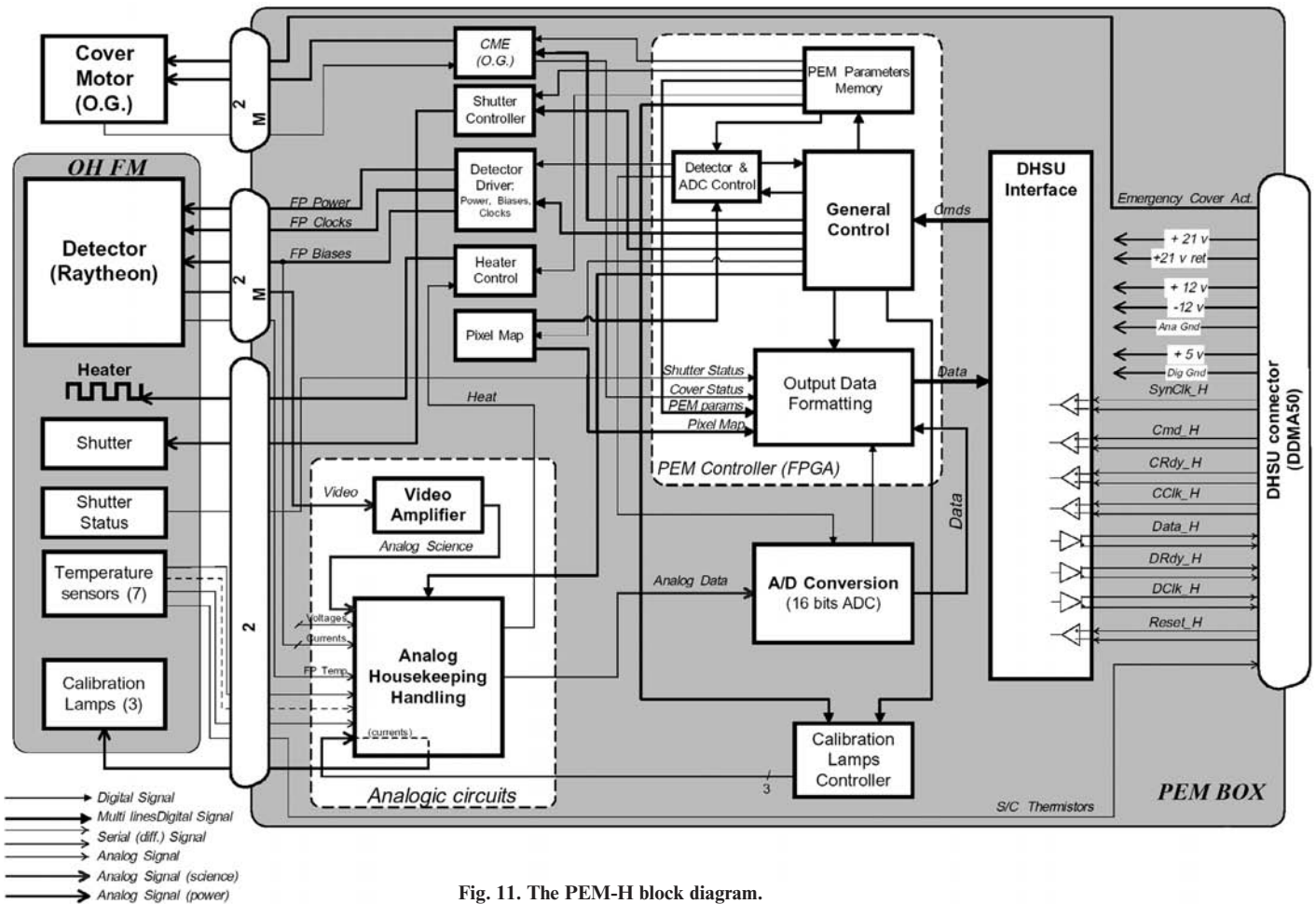


Fig. 11. The PEM-H block diagram.

Thus overall only 15% of the 438 x 270-pixel matrix surface is used. To reduce the overall data rate and volume, VIRTIS-H uses pixel mapping to give the exact location of the spectra over the IR detector. The ME calculates the location of the pixels to be downloaded and passes it to PEM-H, which then downloads them accordingly. The downloaded data are the -H spectra, a set of 432 x 8 x 5. As VIRTIS-H has no spatial resolution, the 5 pixels are averaged together, so the end-product in the nominal acquisition mode is a 3456- (or 432 x 8)-pixel spectrum representing the full spectral range of the instrument from 2  $\mu\text{m}$  to 5  $\mu\text{m}$ .

### 2.5.1 PEM-H

PEM-H, housed in the warm spacecraft environment, contains all the electronics needed to interface the Main Electronics, to drive the FPAs, the shutter and the cover mechanisms and to perform the acquisition and conversion of the science and housekeeping data. The electronics package consists of a mother board and four daughter boards: CME board for the cover control; FPGA board; ADC board; video board. Fig. 11 shows the PEM-H block diagram.

The VIRTIS-H detector has a CMOS-based readout multiplexer. It needs only two Transistor-Transistor Logic (TTL) clocks (main clock and integrate pulse), two power supplies (5 V) and two biases. The Video Amplification and Filtering module amplifies and filters the video signal and sends it to the analogue-digital conversion stage. The Analogue Housekeeping Handling

processes the analogue housekeeping signals (temperatures, voltages and currents), and multiplexes and sends them to the further analogue-digital conversion. This conversion multiplexes the analogue signals (video & housekeeping) and converts them into 16-bit serial data.

The PEM Controller, implemented in an FPGA (ACTEL RT14100), handles the Data Handling and Support Unit (DHSU) commands, the PEM and detector control signals, the PEM and detector clocks and all the input/outputs. The Command Interpreter in the FPGA translates the DHSU commands into PEM commands for further processing.

The PEM Parameters Memory stores the current PEM configuration parameters in the FPGA. Some of these (command bits) are sent directly to the other functions by the PEM Parameters Memory itself.

The Detector and ADC Controller inside the FPGA generates the detector clocks and synchronises accordingly the detector acquisitions by the ADC. The acquisitions are controlled by the Pixel Map, which contains the image of the detector pixels and is used to control the pixel acquisition (only the illuminated pixels are converted). It is written into by the Command Interpreter, controls the Detector & ADC Controller and can be read by the Output Data Formatting. The Output Data Formatting handles the science and analogue housekeeping data (generated by the ADC) and the digital housekeeping data (assigned values and status), formats them and generates the Data Blocks.

The Detector Biases includes four detector bias sources controlled by four DACs. The Calibration Lamps Controller powers the three calibration lamps via three programmable current sources (three DAC channels). A Shutter Controller controls and adjusts shutter closing by means of a programmable current source (one DAC channel). A Cover Controller (CME) controls the cover device and handles the cover status data. Finally, the DHSU Interface handles the commands and data exchanges with the DHSU: unidirectional control signals and serial synchronous data (RS422), PEM synchronisation clock at 8 MHz and Reset control signal. The electronics boxes are shown in Fig. 12.

### 2.5.2 VIRTIS-H IR detector

The VIRTIS-H IR detector is identical to the -M detector but has different filters. The filter window eliminates/reduces the background thermal radiation owing to the temperature of the instrument housing.

Its transmittance characteristics are optimised for each corresponding detector position. The window has an anti-reflection coating optimised in the 2–5  $\mu\text{m}$  region. Two segment filters are coated on to the window with the following passbands:

- 1st region: 2.0–4.4  $\mu\text{m}$ ;
- 2nd region: 3.9–5.0  $\mu\text{m}$ .

### 2.5.3 VIRTIS-H modes

The possible modes for VIRTIS-H are:

*H\_Nominal\_Observation.* The Pixel Map is used to select the region of the IR detector to be downloaded to -ME.

*H\_Calibration.* Start of a calibration sequence.

*H\_Nominal\_Simulation.* Data structure is as for *H\_Nominal\_Observation* but the data content is simulated by the FPGA.

*H\_Science\_Backup.* Full window reading of the IR detector (270 x 438 pixels)

*H\_Spectral\_Calibration\_Simulation.* An *H\_Image\_Slice* (same size as *H\_Science\_Backup* but only simulated data) is delivered to the ME.

*H\_Test.* Test mode to command directly the PEM-H without any ME filter.



Fig. 12. The VIRTIS electronics boxes shortly before integration at IAS Orsay, Paris, during the calibration campaign at the beginning of 2004. The main electronics are at top, PEM-H is at left and PEM-M is at right.

#### 2.5.4 Data reduction tool for VIRTIS-H analysis

A software web tool was developed to provide a quick-look facility for all Co-Investigators. The tool can:

- change the displayed frame (if the Planetary Data System file contains several);
- change the contrast and the colouring scheme;
- draw horizontal and vertical profiles by clicking on the picture;
- compute the spectra for selected orders; if necessary, it can change the pixel map used.

If a more sophisticated treatment is needed, the data must be downloaded to a dedicated machine. A ‘VIRTIS Virtual Instrument’ tool was built to simulate observations for a source whose flux is described by the user. The goal was to help the Co-Investigators to prepare the observations to be performed with the real VIRTIS instruments.

### 2.6 Main Electronics

The Main Electronics are physically separated from the Optics Module and the Proximity Electronic Modules (Fig. 12).

The ME consists of two Data Processing Units (DPUs), including the spacecraft interface electronics and the related power supply units, the power supply for VIRTIS-M/H, and the VIRTIS-M/H interface electronics (M/H IFE), which include the respective Cooler Controller Electronics (CCE) and Cover and cooler Switching Electronics (CSE) and the M/H reference clock generator (MCLK/RCLK). The DPUs, spacecraft interfaces and VIRTIS-M/H interfaces are also known as the Data Handling and Support Unit.

There is a cold-redundant DPU, with the respective redundant power supply unit and redundant common clock generators.

To power the VIRTIS-M/H subsystems, there is only one supply unit. It is not redundant owing to the logical redundancy of the two VIRTIS-M and -H channels (heritage from Rosetta). If the main DPU or main power supply unit (main channel) fails, the redundant channel (redundant DPU and power supply unit) can be switched on by the spacecraft redundant power interface.

The cross-strapping between the two VIRTIS-M and -H subsystems and the main or redundant channel (power supply and DPU) is implemented in the ME M-IFE and H-IFE. An additional cross-strapping is implemented to provide the +28 V input power for the VIRTIS-M/H power converter. The VIRTIS-M/H interface electronics (M/H-IFE) are supplied by the main or redundant DPU power. The resulting power is distributed by respective switches in order to turn on or off the VIRTIS-M/H IFE separately.

The VIRTIS subsystems (VIRTIS-M, -H, coolers and covers) are switched on/off via telecommands and controlled by the DHSU.

For controlling the two coolers (inside the OM), two electrically independent CCEs are located in the ME box and can be switched on or off by the respective +28 V CSE and controlled by the DPU via the M/H-IFE.

The DHSU provides the platform for the data processing/handling and the instrument-control functions, which are performed by software. The main tasks of the DHSU are:

- acquisition, pre-processing, compression and formatting of the science and calibration data of VIRTIS-M and -H subsystems;
- control and power switching of VIRTIS-M, -H (including the electromechanical devices, the scan mirror for -M and shutters), the coolers and covers;
- health check of the instrument and the operational status of VIRTIS to the spacecraft;

- execution of up/downlink activities to and from VIRTIS;
- interpretation, execution and acknowledgement of telecommands;
- management and synchronisation of activities between VIRTIS and the spacecraft.

The data-processing and the data-handling activities by the DHSU are performed on-line. The DHSU communicates with VIRTIS-M, VIRTIS-H and the spacecraft via serial interfaces and an ME common bus, which is separated from the local bus of the DPU.

Each DPU has a high-speed data interface to the Solid-State Mass Memory (SSMM), a low-speed telemetry interface (TM I/F) and low-speed telecommand interface (TC I/F) to the Remote Terminal Unit (RTU).

All interfaces are handled by interrupt, in order to decouple the asynchronous processes between the DPU and the interfaces and to put the DPU in a power-down mode while not operating.

Data processing and handling are sub-slice-oriented (a sub-slice is a 64 pixel x 144 or 64 x 72 spectels). The 16-bit organised data from VIRTIS-M and -H are transferred via serial interfaces, FIFO (First-In, First-Out) buffer and common bus into the local data memory of the DHSU. This data acquisition process is performed in the background, while the processor completes the processing of data from previous exposures. The DPU performs the data processing, including data compression and telemetry packing. The steps and the kind of data processing and instrument control are defined by special operation modes selected by telecommands.

After processing and compression, the scientific and housekeeping data are formatted and transferred to the FIFO buffer of the spacecraft data interface.

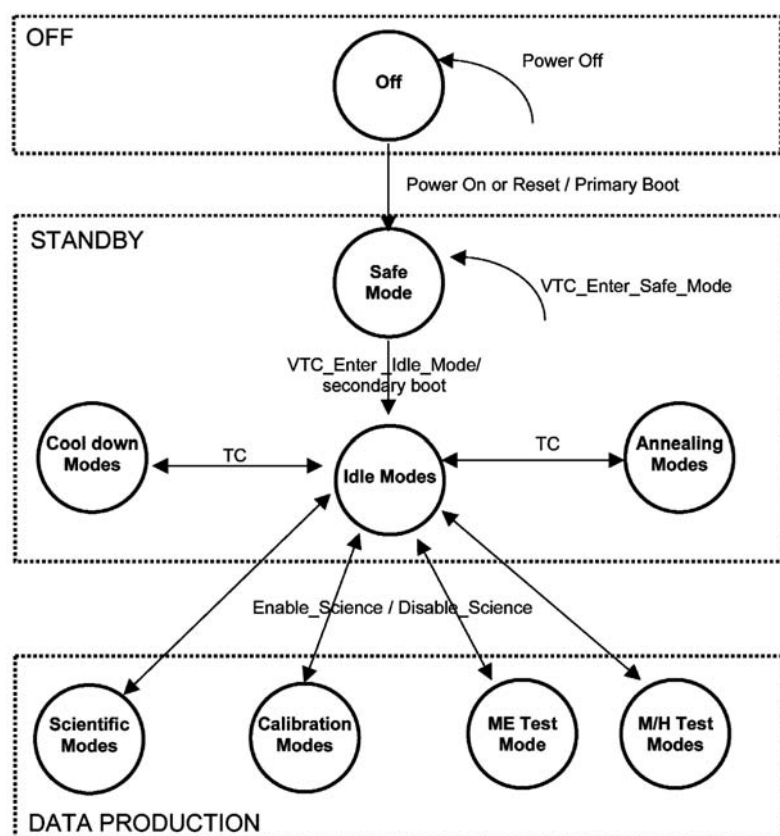


Fig. 13. VIRTIS mode transitions. Once the primary boot is executed, VIRTIS enters safe mode, where only a few commands can be executed. One of these is the 'enter idle' mode, from where it can be operated in full. TC: telecommand. VTC: VIRTIS telecommand.

The interface hardware controls the transfer of the serial block data to the spacecraft (SSMM or RTU).

The DHSU also controls and monitors the status of the different subsystems, including the DHSU itself. The operational housekeeping data are periodically acquired and transferred via the spacecraft low-speed telemetry interface.

A low-power and radiation-hardened Digital Signal Processor (DSP, TSC 21020) is used for the DPU with a computing power of about 20 MIPS.

The DPU memory is divided into three sections: program code; program data; and image data. The program memory consists of the PROMs, EEPROMs and SRAMs. The program code for execution of the Safe Mode is stored in the radiation-hardened PROM and is downloaded by primary boot after power-on to the fast and low-power program SRAM, also radiation-hardened (Fig. 13).

The EEPROM stores the main part of the application software and parameters. The EEPROM content and the Program Memory RAM content can be uploaded by telecommand and downloaded by sending telemetry packets. The validity of the EEPROM content is verifiable by checksum, which is read before secondary boot. The checksum and other status data are stored three times in physically independent configuration areas of the EEPROM. An image data memory stores the raw science data and the intermediate products. The architecture of the DPU has a watch-dog to detect program lockups and endless loops.

#### *2.6.1 DPU*

The core of the DPU is the DSP TSC21020E. It is a high-reliability version of the ADSP21020 and is functionally compatible with this DSP. The DPU communicates with the VIRTIS-M and VIRTIS-H subsystems by serial command/data interfaces. It provides the IEEE-1355 high-speed science data interface (HS link) to the spacecraft SSMM, the low-speed data (SDT) interface for the transfer of housekeeping and the Memory Load Command (MLC) interface to the RTU for VIRTIS telecommanding by the spacecraft or to the EGSE/Spacecraft Interface Simulator (SIS) for on-ground tests. Internally, the DPU controls all other ME units, using separate low-speed serial or parallel interfaces.

The main functionality of the DPU is concentrated around the DSP, which provides computational resources and control capabilities. The DSP operates at 20 MHz, yielding 40 MFLOPs (typical) to 60 MFLOPs (peak) processing power. A further key function is the high-speed serial link communication, which is realised by an IEEE-1355 ASIC (SMCS332). The SMCS332 has three IEEE-1355 full-duplex links (two are used for VIRTIS) that execute data transfers with low Central Processing Unit intervention. Each of the links supports high-level protocol-handling running full-duplex at up to 200 Mbit/s. For VIRTIS only two links with a maximum speed of 10 Mbit/s are used, one for the transfer of scientific data to the SSMM, the other for interacting with a controlling Host PC for development and verification purposes.

The DPU local memory concept is based on a fast static RAM. It provides 128 kword (48-bit) program memory, for 512 kword (40-bit) data memory and 8 kword (16-bit) dual-ported communication memory. The communication memory provides bidirectional buffering between the local processor and the SMCS332. It decouples the different speed characteristics of the DSP and the communication link.

The DPU Extension Board is an extension unit for the DPU that contains only VIRTIS-specific functionalities. These are the On-Board Data Handling (OBDH) interfaces, a data memory extension, an EEPROM bank, internal interfaces to other ME units and additional control logics located in an ACTEL FPGA. Reading the status of the DPU Extension Board, as well as writing the configuration of the local resources, is managed by simple memory accesses of the TSC21020E.

A 2 M x 16-bit image memory extension is used for intermediate buffering of

the spectral data before compression. A 1024 K x 8-bit EEPROM memory provides non-volatile storage of program code and mode parameters. The EEPROMs are only switched-on/off during the secondary boot load of EEPROM content into the Program Memory in order to minimise radiation influences during VIRTIS mission operation. The necessary separation of the EEPROM lines from the DPU busses is realised by additional bus drivers in order to avoid power loading conflicts.

Serial 16-bit unidirectional interfaces to the spacecraft (MLC and SDT) are used for telecommand and telemetry transmission from and to the spacecraft. TM and TC data are buffered by two separate 8 K x 9-bit FIFOs.

### 2.6.2 Software

The PROM software is hard-coded in the Main Electronics/DPU and the EEPROM software is changeable by memory upload (memory management service). The PROM software is written in Assembler, it has a size of 5139 48-bit instructions and consists of 66 modules.

After Primary Boot the PROM software runs using only the Program Memory for safety reasons. Fig. 13 shows a state block diagram.

Primary Boot is performed by the DPU Board and Boot Controller (BBC) after +28 V power-on. The PM has a very good Single Event Upset (SEU) performance (almost SEU-free) while the Data Memory (DM) is SEU-sensitive. Safe behaviour of all PROM software functions can therefore be assumed.

The EEPROM software is stored in EEPROM as PM and DM segments with segment checksum for verification during upload and start (i.e. Secondary Boot from EEPROM in RAM). It runs in PM and DM RAM. The EEPROM software is mainly written in C with low-level functions in Assembler for speed and code optimisation. The VIRTUOSO Real Time Operating System (RTOS) is used and 51 processes can be active simultaneously.

The Secondary Boot software consists of about 200 functions, excluding VIRTUOSO functions/library (VIRTUOSO V4.1 R2.05 is used). The size of the secondary boot software is about 83 Kwords with 68 K Instructions and 15 K Program data/parameter. The compressed code stored in EEPROM is 354 Kbyte (about 60 Kwords). This means that two executables can be stored in EEPROM from the size point of view. Generally, about 170 K of Instructions can be stored in EEPROM at maximum and up to eight different executables.

### 2.6.3 Data compression

Data compression is done for reducing the telemetry data volume either by lossless or lossy compression. A compression unit is always a 144 x 64-element sub-slice. The compression is applicable for VIRTIS-M IR, -M VIS and -H using the same algorithms, depending on the operational parameters.

The reversible algorithm (lossless) is derived from that developed for the OMEGA/Mars Express and VIMS/Cassini imaging spectrometers. It takes advantage of spatial/spectral correlations for pre-processing, then a Rice coding is applied on the residuals. It was mainly used for validation purposes early in the mission and it provides typical compression ratios of 2–4 depending on the entropy content of the data.

The lossy algorithm is based on wavelet transforms. The following compression modes with related factors are applicable:

- lossless compression is data compression without any loss. A differential algorithm is performed with Rice encoding. The compression factor is low (about 1.5) for very noisy M-PEM IR data up to high (about 14) for synthetic IR ramp data. The nominal average compression factor is about 2–4.
- wavelet F1 compression is 'low' lossy. The data compression factor is 8 (2-bit/16-bit).

- wavelet F2 compression is ‘medium’ lossy. The data compression factor is 10.67 (1.5-bit/16-bit).
- wavelet F3 compression is ‘high’ lossy. The data compression factor is 16 (1-bit/16-bit).

### 2.7 Instrument budgets

The total mass of the instrument including internal harness is 33 kg. Total power during science operations is about 50 W. During the cool-down of the IR detectors a long peak of 70 W can be reached even though it is strongly dependent on the thermal environment conditions of the Cold Boxes and baseplate.

The data-rate range is obviously very wide, depending on which mode is being used for observations. As an example, a typical rate of 600 kbit/s is generated for the high resolution when a lossless compression is used, considering an average compression factor of 3 and a repetition time of 2.5 s. The data rate engages mostly the SSMM, while the RTU is used only for the science housekeeping.

In case of failures on both fast interface channels, science data can be transmitted in a degraded mode via the slower OBDH interface.

## 3. Calibration

An intense calibration campaign was performed early on at the subsystem level for VIRTIS-M and -H (Drossart et al., 2004) and then at the system level at the large facility in IAS Orsay (F). VIRTIS carries several internal calibration devices in order to check the spectroscopic and radiometric parameters from time to time during the mission.

### 3.1 Ground calibration

All the FM detectors were tested and calibrated separately in an *ad hoc* facility in advance of installation (Fig. 14). The main parameters were measured at 60K, 70K, 80K, and 100K, and different wavelengths when relevant:

- dark current without spectrometer background;
- charge response (linearity);
- photon flux response (linearity);

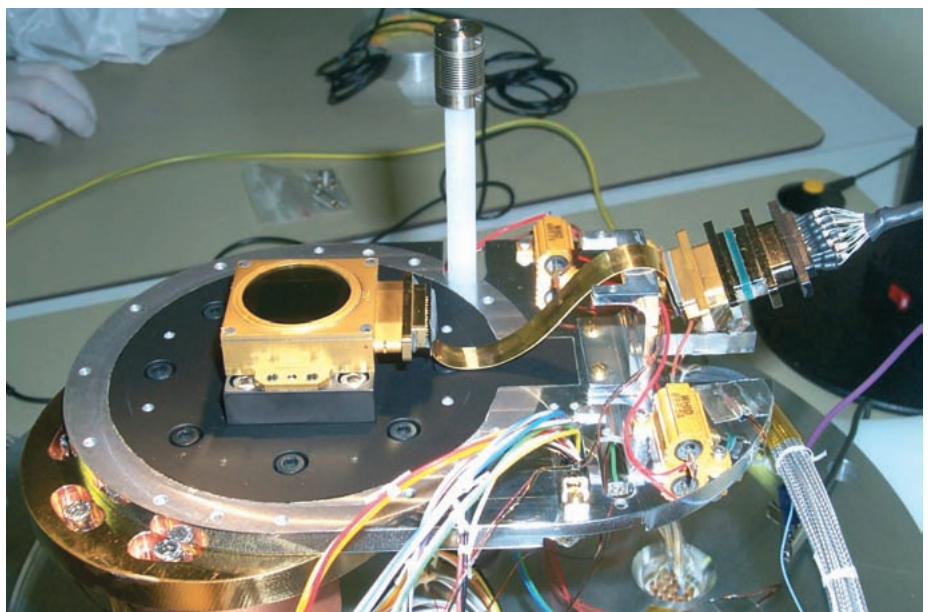


Fig. 14. The VIRTIS-H detector on the calibration bench before integration.

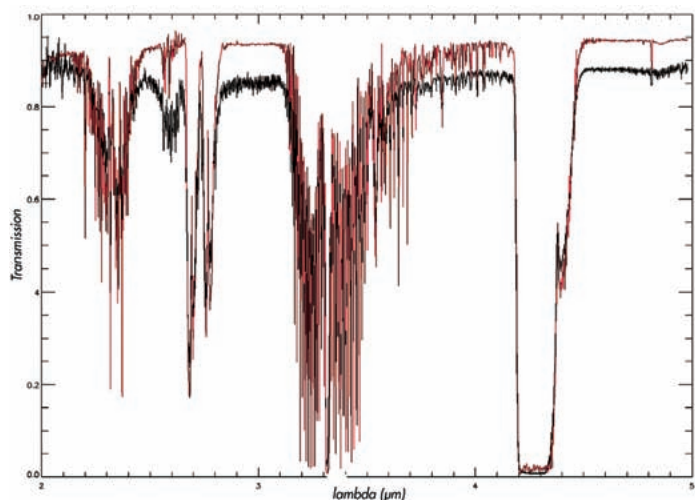


Fig. 15. Gas-cell transmission measured with VIRTIS-H (black curve) compared with the same cell measured by a laboratory FTS (red curve).

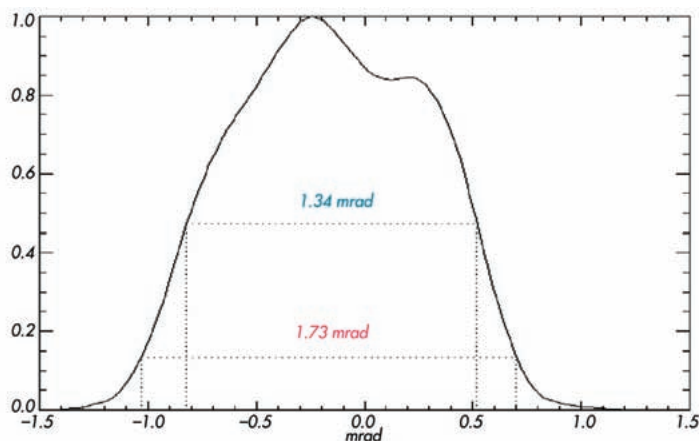


Fig. 16. VIRTIS-H spatial profile along the spatial direction (parallel to the -M slit). The FWHM of IFOV along the slit is 1.34 mrad (about 5–6 high-resolution pixels of -M). In the cross-slit direction, the FWHM is about 0.44 mrad (about 2 high-resolution pixels of -M).

- flat fields;
- readout noise;
- blooming effects.

A dedicated irradiation test was performed on a test-detector to verify its behaviour over the required life. The conditions were:

- proton flux at 180K at: 20 MeV, 30 MeV, 40 MeV and 50 MeV;
- bombardments up to  $2 \times 10^{10}$  particles/cm<sup>2</sup> on a single chip detector.

The dark current showed a variation of less than 1% after the irradiation tests, illustrating the detector's robustness.

VIRTIS underwent several calibration sessions, performed with different Cold-Box temperatures, devoted to spectral and spatial calibration, radiometric calibration, geometric calibration, internal calibration and co-alignment measurements, among others.

A monochromator was used to measure the spectral registration and calibration. For VIRTIS-H, an average of 10 evenly-distributed wavelengths was recorded per grating in order to interpolate the spectral resolution. Owing to the use of the grating's high orders, the spectral resolution varies significantly along the orders. The specification of an average resolution of 2000 around 3.3  $\mu\text{m}$  was achieved. CO<sub>2</sub> and CH<sub>4</sub> gas cells and mineral samples were used for spectral registration of real targets for both VIRTIS-M and -H. Fig. 15 shows the spectrum of the gas cell measured with VIRTIS-H compared with that measured on a laboratory Fourier Transform Spectrometer.

For the VIRTIS-M spectral profile measurement, a scan about the centre of the slit was performed by a monochromator using a wavelength step of the order of 1/5 of a spectel. The resulting Full Width at Half Maximum (FWHM) is 2 nm for visible and 11 nm for IR.

To measure the spatial IFOV, the slit was scanned in the spatial direction with a pinhole. Fig. 16 shows the FWHM and expected width for VIRTIS-H. Considering a pupil diameter of 32 mm, the etendue is  $\sim 0.6 \times 10^{-9}$  m<sup>2</sup> sr at FWHM of the FOV and  $0.8 \times 10^{-9}$  m<sup>2</sup> sr at 18% of the full maximum of the FOV. At FWHM, the VIRTIS-H IFOV along the slit is 1.34 mrad.

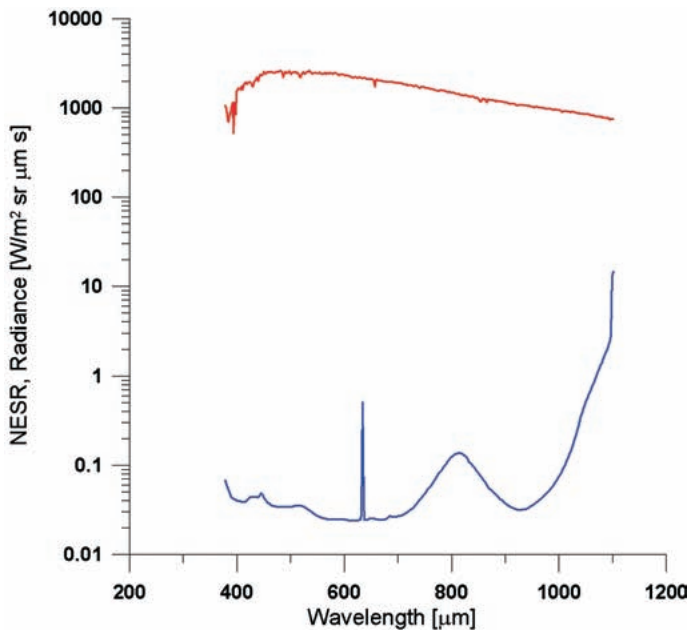


Fig. 17. The NESR of VIRTIS-M visible (blue) compared with a typical modelled radiance of the Venus dayside (red) with nadir-viewing. The NESR is obviously well below the bright radiance from the dayside, so there is a good SNR for short exposures of a fraction of a second. The ratio is essentially limited by the dynamic noise of the analogue-digital converter.

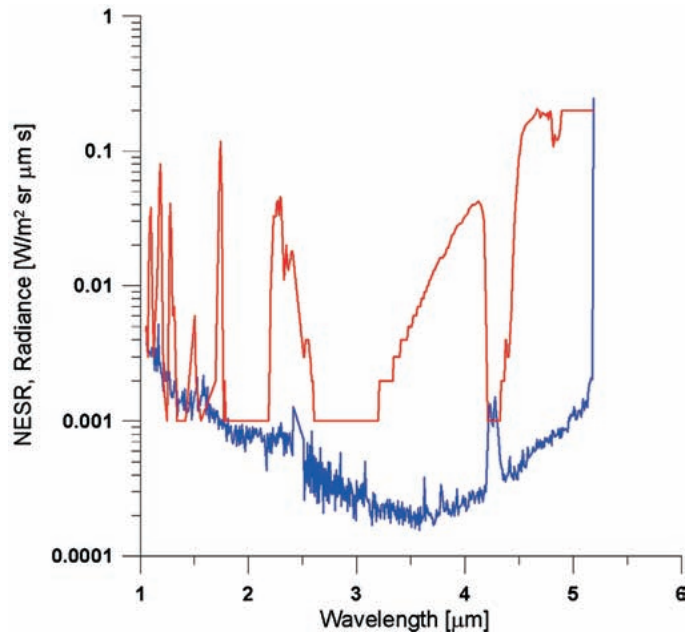


Fig. 18. The NESR of VIRTIS-M IR (blue, lower curve) measured at 135K for the Cold Boxes, compared with the modelled weak radiance from the Venus nightside (red, upper curve) with nadir-viewing. The NESR is well below the expected radiance, thus VIRTIS is able to detect most of the radiance escaping from the planet. The thermal background is not considered here; it depends strongly on the temperature of the Cold Boxes.

The VIRTIS-M spatial profile is bi-dimensional, one direction being along the slit (the ‘pixel’ function) and the other across the slit (the ‘slit’ function). The visible and IR FWHMs are similar and close to the spatial sampling of  $250 \mu\text{rad}$ . The -M visible slit function is also similar to the nominal spatial sampling along the scan direction ( $250 \mu\text{rad}$ ), while the IR equivalent is slightly worse by a factor of two.

To measure the VIRTIS-H defocusing and image quality, a pinhole was used at several wavelengths with a Hartmann mask near the entrance pupil. For each position of the mask, an image was recorded and the position of the impact estimated by gaussian fit. The set of positions allowed an estimate of the wavefront to be reconstructed. At  $3.4 \mu\text{m}$  the measured wavefront error is about  $\lambda/5\text{RMS}$ , showing that the spectral resolution is not reduced by the image quality.

From a radiometric point of view, a blackbody at different temperatures was used to estimate the sensitivity of VIRTIS in terms of flux. The setup was placed in a neutral nitrogen environment to remove atmospheric absorptions. Images were recorded and the spectrum reconstructed for each blackbody temperature (600, 460, 455, 451,  $450^\circ\text{C}$ ). The linearity of the response at  $4.4 \mu\text{m}$  allowed the temperature variations to be measured to better than half a degree. The maximum relative deviation to linearity is less than 0.06%.

For the VIRTIS-M radiometric performance and Noise Equivalent Spectral Radiance (NESR), see Figs. 17 and 18 and Section 4.

### 3.2 In-flight calibration

VIRTIS-M uses two custom lamps optimised for the respective visible and IR channel (Melchiorri et al., 2003). Nevertheless, the lamps can be seen by both channels, providing redundancy. The lamp illuminates the internal part of the -M

cover, designed to reflect the radiance diffusely back towards the instrument. The cover has two areas of different materials chosen to have higher spectral reflectance for the lamp and the related channel. The areas correspond roughly to the visible and IR part of the instrument pupil. This choice comes from a trade-off between the mechanical constraints and the need for the best calibration. The lamp's spot size is equal to the pupil dimension and also spatially homogeneous at the distance of the cover.

The lamps are highly stable and an intense qualification campaign was carried out on the qualification lamps while checking the limited degradation with time. Two different filters in front of the lamp window checked the spectroscopic performances: an Holmium filter for the visible lamp and a polystyrene filter for the IR.

For VIRTIS-H, two spectral and one radiometric internal calibration modules are used in the spectrometer. The spectral calibration module uses a tungsten lamp and a temperature-calibrated Fabry-Pérot that gives 20–10 lines depending on the grating order. One of the modules is used through the entrance cover mirror that returns the flux to the telescope and slit. The other is used through the back of the slit that returns the flux to the collimator. The radiometric calibration module uses a tungsten lamp through the entrance cover mirror.

This Fabry-Pérot system allows the spectral registration of the instrument to be confirmed after a shift is suspected, for example, following the vibrations induced by launch. The absolute position of each known spectral line on the detector is gauss-fitted for each order and used to reconstruct the spectral registration of the instrument to a 2-degree polynomial function. Those functions are then used to give the correspondence between the pixel number and the wavelength for each pixel.

The predicted radiometric performance at Venus is good enough to work with short exposure times (and thus high repetition time). This achieves the scientific objectives not only for the dayside but also for the nightside, where the radiance is very weak. From the expected DN rate for the VIRTIS-M visible channel when looking at the dayside using nadir geometry, the maximum exposure time to avoid saturation is 0.36 s.

For the nightside, the predominant factor is the lack of photons. From the expected DN rate for VIRTIS-M IR over the nightside, the maximum usable exposure time is 4.5 s.

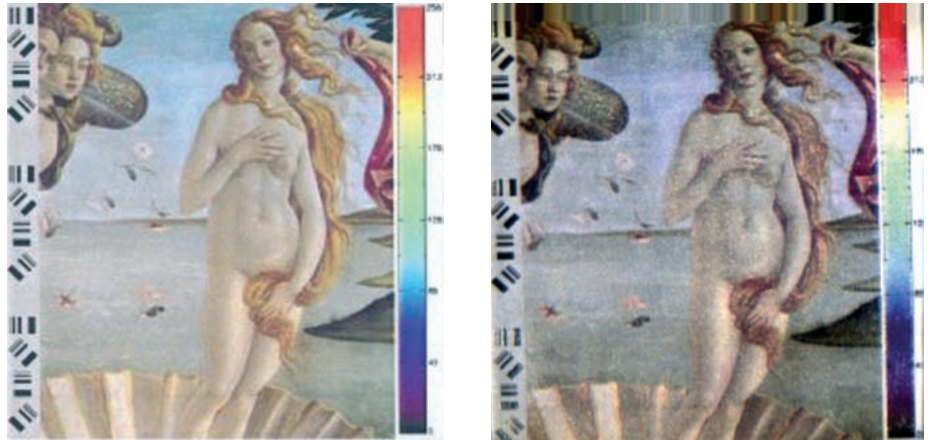
The actual maximum integration time will be limited by the background (depending on the temperature of the Cold Box) rather than the flux from Venus. The typical value for the exposure is significantly less than 4.5 s. A typical exposure time of 1 s for nadir-viewing is used for -M in order to avoid saturation at wavelengths longer than 4.2  $\mu\text{m}$ . The temperature of the Cold Box may in this sense dramatically affect the thermal background, especially at the longest wavelengths. The saturation of the thermal region and thus a larger integration time is acceptable when the scientific objectives from time to time do not require the wavelength region above about 4.2  $\mu\text{m}$ .

The NESR is a very useful figure for predicting the SNR during the observations. The NESR is given by the ratio of the noise sigma (referred to 1 s exposure time) and the Instrument Transfer Function (responsivity). An equivalent source having a radiance equal to the NESR gives a signal equal to the noise; in other words, an SNR of 1. Fig. 17 shows the NESR of the VIRTIS-M visible channel compared with a typical modelled dayside radiance with nadir geometry. Obviously, there is no SNR problem for the dayside, as the NESR is well below the radiance. This is also true for VIRTIS-H and -M IR.

Fig. 18 shows the NESR and the expected radiance for VIRTIS-M IR (and similarly VIRTIS-H) using nadir geometry over the nightside. The NESR is well

## 4. Expected Performance

Fig. 19. Example of a true-colour reconstruction. At left is the (rather poor) target, acquired by a computer scanner. At right is the resulting image from the VIRTIS-M visible raw data without any correction. Only three channels (RGB) were used from the 432 bands.



below the expected radiance, so VIRTIS is able to detect most of the weak radiance escaping from the planet.

The ground-spot size is small enough for all the scientific objectives, even at apocentre (66 000 km altitude), where it is about 15 km in high-resolution for VIRTIS-M and about 80 km for -H. The minimum and typical repetition time for all the observations is 2.5 s.

Another important task for VIRTIS-M visible is providing true-colour images for public outreach. During the subsystem calibration campaign, VIRTIS-M visible (and IR, although not shown here) imaged a target placed in the focal plane of the set-up collimator to simulate an image at infinite distance. Fig. 19 shows the result, comparing the original (rather poor) picture and the raw image from VIRTIS. The image uses only raw data; there is no correction for the illuminating lamp, no flat-field correction and only three channels (RGB) were used out of the 432 bands.

## 5. Observations

The following observation cases are being used by VIRTIS at Venus (not in order of priority):

### *Case 1 (pericentre observations)*

These observations are usually made for statistical coverage of different regions of Venus, night and day. The use of the scanning mirror (in fixed or scanning mode) improves the statistical coverage, but image reconstruction is difficult owing to the high speed of the spacecraft (Fig. 20). The pixel size is defined as the linear dimension of the VIRTIS-M high-resolution spatial pixel (250  $\mu$ rad in angle) on the surface of Venus at the centre of the slit. The dwell time is typically less than the minimum repetition time, which means that image reconstruction is not possible, or the pixels are elongated in the direction of motion or there are 'holes' when the -M scanning mirror is used.

Observing the same region at a variety of phase angles ('feature tracking') is essential for characterising the phase function of the scattering particles ( $\text{H}_2\text{SO}_4$ ). The knowledge of the phase function is important for accurate modelling of the scattering in radiative transfer retrievals. It also provides information on the mean particle size.

### *Case 2 (off-pericentre observations)*

These observations allow VIRTIS to perform spectral mapping (for -M) at the best spatial resolution, with image cube reconstruction obtained by internal mirror motion synchronised with orbital motion (an altitude higher than

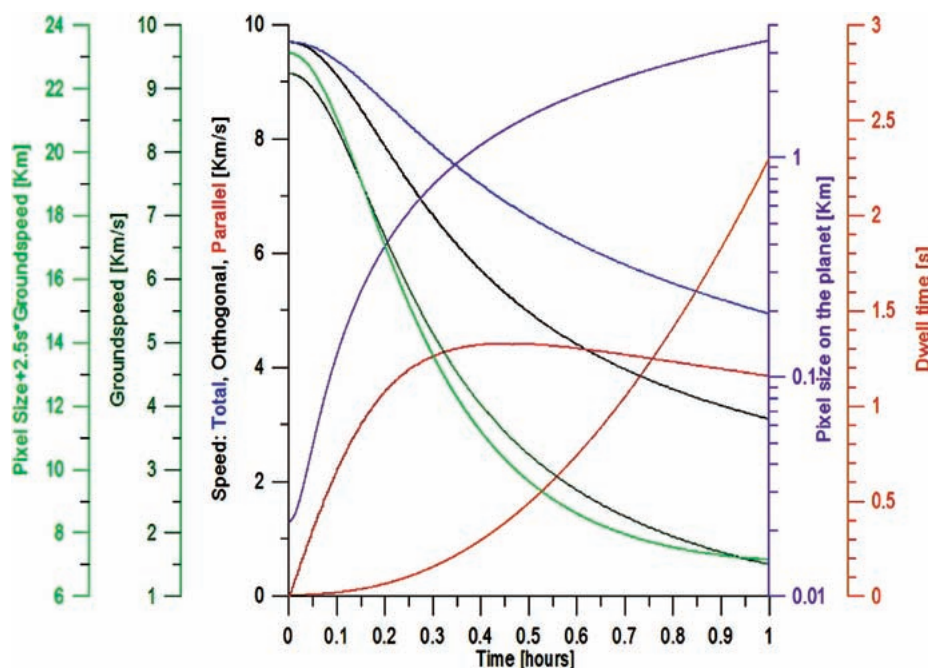


Fig. 20. The main observation parameters for VIRTIS in science Case 1. The colour of each curve and the axis to which it refers are the same. The abscissa is the time along the orbit in hours; time 0 is the pericentre pass of the spacecraft. The plotted parameters are the absolute speed of the spacecraft and its components: along the direction of the observation (component parallel to the optical axis of VIRTIS) and orthogonal to the direction of the observation (perpendicular to the optical axis of VIRTIS). Groundspeed is the spacecraft's relative speed over the surface.

12 000 km is needed). This mode is being intensively used, as most of the scientific objectives related to combined spectroscopic/mapping are obtained in this phase of the orbit.

#### Case 3 (apocentre observation)

This mode allows VIRTIS to observe the full disc of the southern hemisphere, through off-nadir pointing in a mosaic of 3 x 3 images, as shown in Fig. 21. This mode is essential for studying the dynamics for global meteorology; repetition during several orbits provides a full atmospheric rotation. It is also used to map the temperature field, cloud properties, winds and atmospheric chemistry, and it is important for public outreach images.

#### Case 5 (stellar occultation/3-axis stabilisation)

This mode is used in parallel with the SPICAV instrument, which is the driver for this case. VIRTIS is able to retrieve upper atmospheric structure and composition by studying spectral absorption of stellar flux. In particular, minor constituents can be detected, and the upper atmosphere structure is being deciphered from CO<sub>2</sub> absorption. This case is naturally combined from a geometrical point of view with case 7.

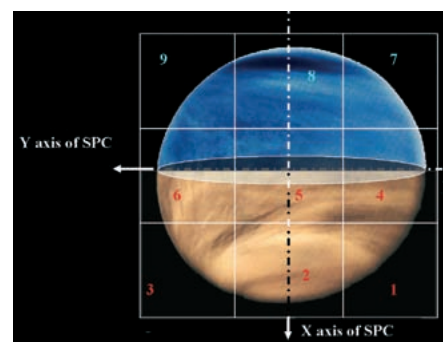
#### Case 7 (limb sounding)

The instrument's unique capability of imaging in the 4.3  $\mu\text{m}$  CO<sub>2</sub> band provides powerful sounding of the mesospheric emissions. Mars Express/OMEGA observations of the Martian limb have provided interesting observations, which VIRTIS is complementing at Venus in a similar observing mode.

Limb observations provide vertical resolution and allow higher altitudes to be probed owing to longer atmospheric paths (at and above cloud tops) up to 115 km, thus reaching the thermosphere ('cryosphere' in this case) where LTE no longer applies.

High priority is given to selected surface targets; the planet's slow rotation offers limited opportunities for each target. Even though nadir or near-nadir viewing (with some off-track or across-track angles) is being used most, feature-

Fig. 21. Spacecraft repointing strategy with numbered sequence for VIRTIS in science case 3 (global mosaic from apocentre). The dark side of Venus is at top and the radiator (-X) is pointed to shadow. The Y axis is parallel to the solar panels. The ellipse at the centre arises from the fact that the ground track at apocentre is at about 80°S and not 90°S according to the actual orbital parameters. VIRTIS can observe the dayside in the visible, and both sides in the IR using two exposure times.



tracking pointing is helping greatly to study the radiance for different phase angles, especially around pericentre, and thus to infer the radiative transfer properties more extensively.

## 6. Conclusions

Venus Express, ESA's second planetary mission, will not solve all the mysteries behind the dense atmosphere. Nonetheless, it is a major step in the long-term systematic exploration of Venus. VIRTIS is playing a significant role in ensuring a high science return from the mission. It is highly desirable that the results from Venus Express triggers a new wave of exploration of our sister planet.

## References

- Allen, D.A. & Crawford, J.W. (1984). Cloud Structure on the Dark Side of Venus. *Nature* **307**, 222–224.
- Artru, J., Lognonné, P. & Blanc, E. (2001). Normal Modes Modeling of Post-Seismic Ionospheric Oscillations. *Geophys. Res. Letters*, **28**, 697.
- Baines, K.H., Bellucci, G., Bibring, J.-P., Brown, R.H., Buratti, B.J., Bussoletti, E., Capaccioni, F., Cerroni, P., Clark, R.N., Coradini, A., Cruikshank, D.P., Drossart, P., Formisano, V., Jaumann, R., Langevin, Y., Matson, D.L., McCord, T.B., Mennella, V., Nelson, R.M., Nicholson, P.D., Sicardy, B., Sotin, C., Hansen, G.B., Ajello, J.J. & Amici, S. (2000). Detection of Sub-micron Radiation from the Surface of Venus by Cassini/VIMS. *Icarus* **148**, 307–311.
- Bézar, B., De Bergh, C., Crisp, D. & Maillard, J.P. (1990). The Deep Atmosphere of Venus Revealed by High-Resolution Night Side Spectra. *Nature* **345**, 508–511.
- Bibring, J.-P., Langevin, Y., Poulet, F., Gendrin, A., Gondet, B., Berthé, M., Soufflot, A., Drossart, P., Combes, M., Bellucci, G., Moroz, V., Mangold, N., Schmitt, B. & the OMEGA team (2004). Perennial Water Ice Identified Around the Mars South Pole. *Nature* **428**, 627–630.
- Carlson, R.W., Baines, K.H., Encrenaz, Th., Taylor, F.W., Drossart, P., Kamp, L.W., Pollack, J.B., Lellouch, E., Collard, A.D., Calcutt, S.B., Grinspoon, D., Weissman, P.R., Smythe, W.D., Ocampo, A.C., Danielson, G.E., Fanale, F.P., Johnson, T.V., Kieffer, H.H., Matson, D.L., McCord, T.B. & Soderblom, L.A. (1991). Galileo Infrared Imaging Spectroscopy Measurements at Venus. *Science* **253**, 1541–1548.
- Collard, A.D., Taylor, F.W., Calcutt, S.B., Carlson, R.W., Kamp, L.W., Baines, K.H., Encrenaz, Th., Drossart, P., Lellouch, E. & Bezard, B. (1993). Latitudinal Distribution of Carbon Monoxide in the Deep Atmosphere of Venus. *Planet. Space Sci.* **41**, 487–494.
- Coradini, A., Capaccioni, F., Drossart, P., Semery, A., Arnold, G., Schade, U., Angrilli, F., Barucci, M.A., Bellucci, G., Bianchini, G., Bibring, J.P., Blanco, A., Blecka, M., Bockelee-Morvan, D., Bonsignori, R., Bouye, M., Bussoletti, E., Capria, M.T., Carlson, R., Carsenty, U., Cerroni, P., Colangeli, L., Combes, M., Combi, M., Crovisier, J., Dami, M., DeSanctis, M.C., DiLellis, A.M., Dotto, E., Encrenaz, T., Epifani, E., Erard, S., Espinasse, S., Fave, A., Federico, C., Fink, U., Fonti, S., Formisano, V., Hello, Y., Hirsch, H., Huntzinger, G., Knoll, R., Kouach, D., Ip, W.H., Irwin, P., Kachlicki, J., Langevin, Y., Magni, G., McCord, T., Mennella, V., Michaelis, H., Mondello, G., Mottola, S., Neukum, G., Orofino, V., Orosei, R., Palumbo, P., Peter, G., Pforte, B., Piccioni, G., Reess, J.M., Rees, E., Saggin, B., Schmitt, B., Stefanovitch, Stern, A., Taylor, F., Tiphene, D. & Tozzi, G. (1998). VIRTIS: An Imaging Spectrometer for the Rosetta Mission. *Planet. Space Sci.* **46**(9/10), 1291–1304.
- Drossart, P., Bezard, B., Encrenaz, Th., Lellouch, E., Roos, M., Taylor, F.W., Collard, A.D., Calcutt, S.B., Pollack, J. & Grinspoon, D.H. (1993). Search for

- Spatial Variations of the H<sub>2</sub>O Abundance in the Lower Atmosphere of Venus from NIMS Galileo. *Planet. Space Sci.* **41**, 495–504.
- Drossart, P., Piccioni, G., Coradini, A., Réess, J., Sémerly, A., Suetta, E., Cosi, M., Dami, M. & Arnold, G. (2004). VIRTIS Imaging Spectrometer for the ESA/Venus Express Mission. *SPIE Infrared Spaceborne Remote Sensing XII*, Denver, Colorado, USA, 2–6 August 2004.
- Melchiorri, R., Piccioni, G. & Mazzoni, A. (2003). VIRTIS-M Flight Lamps. *Rev. Sci. Instrum.* **74**(8), 3796–3801.
- Kamp, L.W., Taylor, F.W. & Calcutt, S.B. (1988). Structure of Venus's Atmosphere from Modelling of Night Side Infrared Spectra. *Nature* **336**, 360–362.
- Piccioni, G., Amici, S., Fonti, S., Coradini, A. & Dami, M. (2000). Efficiency Measurements of the VIRTIS-M Grating. *Planet. Space Sci.* **48**(5), 411–417.
- Roldan, C., López-Valverde, M.A., López-Puertas, M. & Edwards, D.P. (2000). Non-LTE Infrared Emissions of CO<sub>2</sub> in the Atmosphere of Venus. *Icarus* **147**, 11–25.
- Roos, M., Drossart, P., Encrenaz, Th., Lellouch, E., Bezard, B., Carlson, R.W., Baines, K.H., Kamp, L.W., Taylor, F.W. & Collard, A.D. (1993). The Upper Clouds of Venus: Determination of the Scale Height from NIMS-Galileo Infrared Data. *Planet. Space Sci.* **41**, 505–514.
- Taylor, F.W., Crisp, D. & Bézard, B. (1997). Near-Infrared Sounding of the Lower Atmosphere of Venus. In *Venus II*, Univ. of Arizona Press, Arizona, USA, pp325.